# Quantum theory of Rabi sideband generation by forward four-wave mixing

G. S. Agarwal
*School of Physics, University of Hyderabad, Hyderabad 500 134 Andhra Pradesh, India*

Robert W. Boyd
*Institute of Optics, University of Rochester, Rochester, New York 14627*
(Received 7 December 1987; revised manuscript received 6 June 1988)

The predictions of a quantum-mechanical theory of forward four-wave mixing in a homogeneously broadened system of two-level atoms are presented. In the limit of a very short interaction region, the predictions of this theory reproduce those of well-known theories for the spontaneous-emission spectrum of an atom in the presence of an intense laser field. More generally, the theory predicts how the emission spectrum is modified due to propagation effects for a medium of arbitrary length. For long propagation path lengths, the emitted radiation can be quite intense and has a spectrum that is strongly peaked at the Rabi sidebands of the incident laser frequency. The theory shows that Rabi sideband generation in the forward direction can be understood as parametric amplification of weak radiation emitted spontaneously at the Rabi sidebands. The quantum noise that initiates the four-wave-mixing process has contributions both from fluctuations in the incident vacuum radiation field and from fluctuations in the polarization of the atomic dipoles. Both contributions are important for the case of a radiatively broadened medium, although the material fluctuations make the dominant contribution for the case of a medium in which the broadening is largely collisional. Under certain conditions large amounts of squeezing in the radiated field are predicted.

## I. INTRODUCTION

When an intense, near-resonant laser beam propagates through an atomic vapor, several different quantum-optical processes can occur. These processes include spontaneous emission from the strongly driven atoms and four-wave-mixing effects, which can lead to a dramatic modification of the character of the emitted radiation. For sufficiently large laser intensities, spontaneous emission occurs in the form of a three-peaked resonance fluorescence spectrum, consisting of a central component and of two sidebands symmetrically detuned from the central component by the generalized Rabi frequency.[1,2] Resonance fluorescence is emitted in the form of a dipole radiation pattern, and hence is emitted in nearly all directions. For the case of large path lengths through the atomic vapor, propagation effects become important. These propagation effects can lead to a modification of the spectrum and directionality of the emitted radiation, due both to the possibility of reabsorption of the emitted radiation and to the possibility of amplification of the emitted radiation, which in the presence of strong saturation can occur even for an uninverted atomic system.[3] These propagation effects are most dramatic in the near-forward direction, where phase-matched four-wave-mixing processes can occur,[4] leading to the coupling of the spontaneous emission at the two sidebands.

There have been several experimental studies of the emission processes that occur in the near-forward direction when an intense near-resonant laser beam propagates through an atomic vapor.[5–10] The emitted light is often observed to consist of both an upshifted and a downshifted component, with the lower-frequency component often being emitted in the form of a ring surrounding the transmitted laser beam. It has been speculated that this emission results from a four-wave-mixing process that amplifies the radiation spontaneously emitted by the atoms.[9] A semiclassical calculation shows that four-wave-mixing processes lead to significant gain at the two Rabi sidebands, which is also where two of the peaks of the resonance fluorescence spectrum occurs.[4] This radiation is emitted most efficiently in those directions for which the phase-matching condition is achieved.[10] While this semiclassical description presents an appealing explanation of the nature of the conical emission process, it cannot accurately predict the spectrum of the emitted radiation nor can it describe how the four-wave-mixing process is initiated quantum mechanically.

The present paper presents a theoretical treatment of the emission processes of an atomic system when both spontaneous emission and four-wave-mixing processes can occur. While the quantum-mechanical theory of single-atom spontaneous emission and the semiclassical theory of four-wave mixing are well understood, only very recently has four-wave mixing been discussed from a quantum-electrodynamic point of view.[11–17] Our calculation is based on the application of a recently published quantum theory of nonlinear mixing processes involving multimode fields.[16] The results reduce to those of single-atom spontaneous emission in the limit of short propagation pathlengths, but go beyond these results by showing how the spontaneous-emission spectrum is modified by propagation effects. Our calculation shows how the spectrum of the emitted radiation evolves continuously from that of single-atom resonance fluorescence as the path length through the atomic vapor is increased. Our calculation also shows that, for certain values of the propagation path length and of the laser intensity and detuning

 

from resonance, the emitted radiation, obtained by superposing the fields at the two Rabi sideband frequencies, has strong squeezing characteristics. Related calculations have recently been presented by Sargent and coworkers[11–13] and by Reid and Walls.[14,15] These calculation are based on different theoretical formalisms, and one of our motivations is to compare the results of our formalism with theirs. As we show explicitly below, these different formalisms give consistent results. However, our formalism allows us to distinguish between the effects of quantum noise in the incident vacuum field and quantum noise in the response of the material system.

## II. THEORY

The theory of nearly degenerate, forward four-wave mixing used in our calculation is a special case of a recently developed general quantum-mechanical theory of multiwave mixing.[16] We describe the interaction between the atoms and the fields in the electric dipole approximation through the interaction Hamiltonian

$$H_1=-\int \mathbf{P}(\mathbf{r})\cdot\mathbf{E}_p(\mathbf{r},t)d^3r-\int \mathbf{P}(\mathbf{r})\cdot\mathbf{E}(\mathbf{r},t)d^3r\ , \tag{1}$$

where we treat the pump field

$$\mathbf{E}_p(\mathbf{r},t)=\boldsymbol{\epsilon}_p e^{i\mathbf{k}\cdot\mathbf{r}-i\omega t}+\text{c.c.} \tag{2}$$

as a classical quantity but describe the probe field in terms of the quantum-mechanical operator $\mathbf{E}(\mathbf{r},t)$. We assume that the probe field consists of a signal component of frequency $\omega_s$ and a conjugate component of frequency $\omega_c=2\omega-\omega_s$, so that the probe field operator can be represented as

$$\mathbf{E}(\mathbf{r},t)=(\beta_s\boldsymbol{\epsilon}_s a e^{i\mathbf{k}_s\cdot\mathbf{r}-i\omega_s t}+\beta_c\boldsymbol{\epsilon}_c b e^{i\mathbf{k}_c\cdot\mathbf{r}-i\omega_c t})+\text{H.c.}\ , \tag{3}$$

where $a$ and $b$ denote the annihilation operators for the signal and conjugate fields and where we have introduced $\beta_\alpha=-i(2\pi\hbar\omega_\alpha/V)^{1/2}$, for $\alpha=s,c$, $V$ denoting the quantization volume. The polarization operator is expressed in terms of the dipole moment operator $\mathbf{d}^{(i)}$ of an atom located at position $\mathbf{R}^{(i)}$ as

$$\mathbf{P}(\mathbf{r})=\sum_i \delta(\mathbf{r}-\mathbf{R}^{(i)})\mathbf{d}^{(i)}\ . \tag{4}$$

We next assume that the applied and generated field frequencies are sufficiently close to the atomic resonance that the rotating-wave approximation can be used. In this case the Hamiltonian (1) simplifies to

$$H_1=-\int d^3r\,\mathbf{P}^-(\mathbf{r})\cdot[\mathbf{E}_p^+(\mathbf{r},t)+\mathbf{E}^+(\mathbf{r},t)]\ \text{H.c.}\ , \tag{5}$$

where the superscripts + and − designate the positive- (e.g., $e^{-i\omega t}$) and negative- (e.g., $e^{i\omega t}$) frequency parts of the fields, respectively.

The density operator $\rho$ for the coupled atom-field system obeys the equation

$$\frac{\partial\rho}{\partial t}=-\frac{i}{\hbar}[H_{0A}+H_{0F}+H_1,\rho]+L_A\rho\ , \tag{6}$$

where $H_{0A}$ and $H_{0F}$ represent the unperturbed Hamiltonians of the atoms and field, respectively. The effects of spontaneous emission and of collisions are contained in the relaxation Liouville operator $L_A$ of the atoms. Our primary interest is in determining the dynamical behavior of the optical field. For this purpose, we need the field density operator $\rho_F$, which is related to the complete density operator by tracing over the atomic variables:

$$\rho_F=\text{Tr}_A\,\rho\ . \tag{7}$$

The dynamical equation for $\rho_F$ can be obtained using projection-operator techniques. We assume that the probe field is sufficiently weak that we need to retain only the lowest-order nonvanishing terms in the probe operator. The derivation of the field equation of motion involves extensive algebraic manipulations, which are described in Ref. 16. This procedure leads to the master equation

$$\begin{aligned}\frac{\partial\rho_F}{\partial t}=&-\frac{\beta_s^*\beta_c^*N}{2\hbar^2}(\hat{Q}_{sc}^{++}(-i\nu_c)[a^\dagger,[b^\dagger,\rho_F]]+\hat{C}_{sc}^{++}(-i\nu_c)[a^\dagger,\{b^\dagger,\rho_F\}]+\hat{Q}_{cs}^{++}(-i\nu_s)[b^\dagger,[a^\dagger,\rho_F]]\\&+\hat{C}_{cs}^{++}(-i\nu_s)[b^\dagger,\{a^\dagger,\rho_F\}])e^{-it(2\omega-\omega_s-\omega_c)}\\&-\frac{|\beta_s|^2N}{2\hbar^2}(\hat{Q}_{ss}^{+-}(i\nu_s)[a^\dagger,[a,\rho_F]]+\hat{C}_{ss}^{+-}(i\nu_s)[a^\dagger,\{a,\rho_F\}])\\&-\frac{|\beta_c|^2N}{2\hbar^2}(\hat{Q}_{cc}^{+-}(i\nu_c)[b^\dagger,[b,\rho_F]]+\hat{C}_{cc}^{+-}(i\nu_c)[b^\dagger,\{b,\rho_F\}])+\text{H.c.}\end{aligned} \tag{8}$$

Here $N$ denotes the number density of atoms, [,] denotes the commutator, and {,} denotes the anticommutator. The caret denotes the Laplace transform; for example,

$$\hat{C}_{\alpha\beta}^{\pm\pm}(z)=\int_0^\infty d\tau\, e^{-z\tau}C_{\alpha\beta}^{\pm\pm}(\tau)\ . \tag{9}$$

For convenience, we have introduced the signal and conjugate detunings $\nu_s$ and $\nu_c$,

$$\nu_c=\omega-\omega_c,\quad \nu_s=\omega-\omega_s\ . \tag{10}$$

The quantities $C_{\alpha\beta}^{\pm\pm}$ and $Q_{\alpha\beta}^{\pm\pm}$ are linear combinations of the atomic correlation functions $B_{\alpha\beta}^{\pm\pm}$,

$$C_{\alpha\beta}^{\pm\pm}(\tau)=B_{\alpha\beta}^{\pm\pm}(\tau)+B_{\beta\alpha}^{\pm\pm}(-\tau)\ , \tag{11a}$$

$$Q_{\alpha\beta}^{\pm\pm}(\tau)=B_{\alpha\beta}^{\pm\pm}(\tau)-B_{\beta\alpha}^{\pm\pm}(-\tau)\ , \tag{11b}$$

where

$$B^{\pm\pm}_{\alpha\beta}(\tau)=\lim_{t\to\infty}[\langle P^{\pm}_{\alpha}(t+\tau)P^{\pm}_{\beta}(t)\rangle - \langle P^{\pm}_{\alpha}(t+\tau)\rangle\langle P^{\pm}_{\beta}(t)\rangle], \quad (12a)$$

with

$$P^{+}_{\alpha}=\mathbf{P}^{+}\cdot\epsilon^{*}_{\alpha},\quad P^{-}_{\alpha}=(P^{+}_{\alpha})^{*}\ \text{for}\ \alpha=s,c\ . \quad (12b)$$

In Eq. (12), the polarization operator can be evaluated at any point in the medium, as long as the same point is used for $P_\alpha$ and $P_\beta$. The polarization correlations are to be evaluated in the presence of the classical pump field and the Liouville relaxation operator. It is shown in Ref. 16 that the correlation functions $C^{\pm\pm}_{\alpha\beta}$ correspond to the nonlinear susceptibilities that appear in semiclassical theories. The functional form of these susceptibilities is well known for many physical systems; see, for example, Ref. 4 for their form for the case of a two-level system in the presence of saturation effects. The correlation functions $Q^{\pm\pm}_{\alpha\beta}$ have no counterpart in semiclassical theories; they represent the quantum fluctuations of the atomic system. The correlation function $Q^{+-}$ (more precisely, the combination $Q^{+-}-C^{+-}$) can be used to calculate the spectrum of the radiation emitted by a coherently driven system. The correlation function $Q^{++}$ has been referred to as the anomalous correlation function and has been computed for a number of cases;[18] it is useful for calculating the spectrum of the squeezing produced in processes such as resonance fluorescence.[19] Our formulation of the forward four-wave-mixing problem can be shown[20] to be consistent with that of Sargent *et al.*[11] and of Reid and Walls.[20]

For the case of nonlinear mixing by means of the nonlinear response of a two-level atom, the atomic correlation functions can readily be determined. We write the optical Bloch equations for an atom located at position R as

$$\frac{\partial\Phi}{\partial t}=M\Phi+I\ , \quad (13)$$

where $\Phi$ represents the Bloch vector whose components are given by

$$\Phi_1=\langle S^{+}\rangle e^{i\mathbf{k}\cdot\mathbf{R}-i\omega t},\quad \Phi_2=\Phi_1^{*},\quad \Phi_3=\langle S^{z}\rangle\ , \quad (14)$$

where $I$ represents the vector with components

$$I_1=I_2=0,\quad I_3=\eta/2T_1\ , \quad (15)$$

and where $M$ is the matrix

$$M=\begin{bmatrix} -\frac{1}{T_2}+i\Delta & 0 & 2i\Omega^{*} \\ 0 & -\frac{1}{T_2}-i\Delta & -2i\Omega \\ i\Omega & -i\Omega^{*} & -\frac{1}{T_1} \end{bmatrix}. \quad (16)$$

In these equations, $S^{+}$ and $S^{z}$, respectively, represent the polarization and inversion operator for a two-level atom; $T_1$ and $T_2$, respectively, are the population and dipole relaxation times, $\eta$ is the equilibrium population inversion in the absence of the pump field, $\Delta=\omega_0-\omega$, and $\Omega=\mathbf{d}\cdot\epsilon/\hbar$. The polarization field can be determined in terms of the solution to Eq. (13) through

$$\mathbf{P}(\mathbf{r})=\mathbf{d}S^{+}\delta(\mathbf{r}-\mathbf{R})+\text{H.c.} \quad (17)$$

One finds by explicit calculation that the atomic correlation function is given in terms of the steady-state solution of Eq. (13),

$$\Phi=-M^{-1}I\ , \quad (18)$$

and of the elements of the matrix $U$ defined by

$$U(z)=(z-M)^{-1} \quad (19)$$

through the equations

$$\begin{aligned}
\hat{Q}^{++}_{sc}(z)&=(\epsilon_s^{*}\cdot\mathbf{d})^{*}(\epsilon_c\cdot\mathbf{d})\times\sum_l U_{2l}(z)\times(1-2\Phi_1\Phi_2,-2\Phi_2\Phi_2,-2\Phi_2\Phi_3)_l\ ,\\
\hat{C}^{++}_{sc}(z)&=(\epsilon_s\cdot\mathbf{d})^{*}(\epsilon_c\cdot\mathbf{d})^{*}\sum_l U_{2l}(z)(2\Phi_3,0,-\Phi_2)_l\ ,\\
\hat{Q}^{+-}_{ss}(z)&=|\epsilon_s\cdot\mathbf{d}|^{2}\times\sum_l U_{2l}(z)\times(-2\Phi_1\Phi_1,1-2\Phi_1\Phi_2,-2\Phi_1\Phi_3)_l\ ,\\
\hat{C}^{+-}_{ss}(z)&=|\epsilon_s\cdot\mathbf{d}|^{2}\sum_l U_{2l}(z)(0,-2\Phi_3,\phi_1)_l\ .
\end{aligned} \quad (20)$$

We next convert the operator equation (8) to a $c$-number equation by introducing the Wigner distribution function $\phi(z_a,z_b)$ associated with the density matrix $\rho_F$. The Wigner distribution function is defined by

$$\phi(z_a z_b)=\frac{1}{\pi^4}\mathrm{Tr}\left[\rho_F\int d^2\alpha\int d^2\beta\exp\{-[\alpha(z_a^{*}-a^{\dagger})-\alpha^{*}(z_a-a)+\beta(z_b^{*}-b^{\dagger})-\beta(z_b-b)]\}\right], \quad (21)$$

where $\int d^2\alpha$ represents integration over the whole complex $\alpha$ plane. Through use of the Wigner distribution function, the expectation values of symmetrically ordered combinations of operators can be calculated; for example, the expectation value of the number of photons in the signal mode is given by

$$\left\langle\frac{a^{\dagger}a+aa^{\dagger}}{2}\right\rangle=\int d^2z_\alpha\int d^2z_b\,|z_a|^{2}\phi(z_a,z_b)\ . \quad (22)$$

By using the standard rules of mapping associated with Weyl ordering, the master equation can be mapped into the $c$-number equation

$$\frac{\partial\phi}{\partial t}=-\frac{\beta_s^*\beta_c^*N}{2\hbar^2}\left[[\hat{Q}_{sc}^{++}(-i\nu_c)+\hat{Q}_{cs}^{++}(-i\nu_s)]\frac{\partial^2\phi}{\partial z_a\partial z_b}-\hat{C}_{cs}^{++}(-i\nu_c)\frac{\partial}{\partial z_a}(2z_b^*\phi)\right.$$
$$\left.-\hat{C}_{cs}^{++}(-i\nu_s)\frac{\partial}{\partial z_b}(2z_a^*\phi)\right]e^{-it(2\omega-\omega_s-\omega_c)}$$
$$+\left[\left[\frac{|\beta_s|^2N}{2\hbar^2}\hat{Q}_{ss}^{+-}(i\nu_s)\frac{\partial^2\phi}{\partial z_a\partial z_b^*}+\frac{|\beta_c|^2N}{2\hbar^2}\hat{Q}_{cc}^{+-}(i\nu_c)\frac{\partial^2\phi}{\partial z_a\partial z_b^*}+\frac{|\beta_s|^2N}{2\hbar^2}\hat{C}_{ss}^{+-}(i\nu_s)\frac{\partial}{\partial z_a\phi}(2z_a\phi)\right.\right.$$
$$\left.\left.+\frac{|\beta_c|^2N}{2\hbar^2}\hat{C}_{cc}^{+-}(i\nu_c)\frac{\partial}{\partial z_b}(2z_b\phi)\right]+\text{c.c.}\right]. \tag{23}$$

Equation (23) has the form of a linearized Fokker-Planck equation and can be solved using well-known techniques.[16] Note that the correlation functions $C_{\alpha\beta}^{\pm\pm}$, which correspond to semiclassical susceptibilities, appear only in the drift terms, whereas the correlation functions $Q_{\alpha\beta}^{\pm\pm}$, which have no semiclassical counterparts, appear only in the diffusion terms. Hence the deviation of the Wigner function's dynamics from motion on a classical trajectory are due only to the $Q_{\alpha\beta}^{\pm\pm}$ terms which represent the quantum fluctuations of the medium. In fact, it is for this reason that we chose to use the Wigner distribution function for the present calculation. The time evolution of the expectation value of any combination of field operators can be determined in terms of the solution of Eq. (23). For example, we introduce the vector

$$\langle\Psi\rangle=\begin{bmatrix}\langle a\rangle\\ \langle b^\dagger\rangle\end{bmatrix} \tag{24}$$

and the matrix

$$\langle\Psi\Psi^\dagger\rangle=\begin{bmatrix}\langle a^\dagger a\rangle+\frac{1}{2} & \langle ab\rangle\\ \langle a^\dagger b^\dagger\rangle & \langle b^\dagger b\rangle+\frac{1}{2}\end{bmatrix}. \tag{25}$$

The equations of motion for these quantities are then given as

$$\frac{d}{dt}\langle\Psi\rangle=A\langle\Psi\rangle, \tag{26}$$

$$\frac{d}{dt}\langle\Psi\Psi^\dagger\rangle=A\langle\Psi\Psi^\dagger\rangle+\langle\Psi\Psi^\dagger\rangle A^\dagger+2D, \tag{27}$$

where $A$ is the matrix that depends only on $C_{\alpha\beta}^{\pm\pm}$,

$$A=-\frac{N}{\hbar^2}\begin{bmatrix}|\beta_s|^2\hat{C}_{ss}^{+-}(i\nu_s) & \beta_s^*\beta_c^*\hat{C}_{sc}^{++}(-i\nu_c)\\ \beta_s\beta_c(\hat{C}_{cs}^{++})^*(-i\nu)_s & |\beta_c|^2[\hat{C}_{cc}(i\nu_c)]^*\end{bmatrix}, \tag{28}$$

and $2D$ is the diffusive matrix which depends only on $Q_{\alpha\beta}^{\pm\pm}$,

$$2D=\frac{N}{2\hbar^2}\begin{bmatrix}|\beta_s|^2[\hat{Q}_{ss}^{+-}(i\nu_s)+\text{c.c.}] & -\beta_s^*\beta_c^*[Q_{sc}^{++}(-i\nu_c)+\hat{Q}_{cs}^{++}(-i\nu_s)]\\ -\beta_s\beta_c[\hat{Q}_{sc}^{++}(-i\nu_c)+\hat{Q}_{cs}^{++}(-i\nu_s)]^* & |\beta_c|^2[\hat{Q}_{cc}^{+-}(i\nu_c)+\text{c.c.}]\end{bmatrix}. \tag{29}$$

Equations (26) and (27) can be solved to give

$$\langle\Psi(t)\rangle=e^{At}\langle\Psi(0)\rangle, \tag{30}$$

$$\langle\Psi(t)\Psi^\dagger(t)\rangle=e^{At}\langle\Psi(0)\Psi^\dagger(0)\rangle(e^{At})^\dagger$$
$$+2\int_0^t d\tau e^{A\tau}D(e^{A\tau})^\dagger. \tag{31}$$

For the case of present interest in which initially only the pump is acting on the atom, the fields represented by modes $a$ and $b$ are in the vacuum state, and the initial conditions are $\langle\Psi(0)\rangle=0$ and $\langle\Psi(0)\Psi^\dagger(0)\rangle=\frac{1}{2}$. Equations (30) and (31) constitute the complete quantum-mechanical solution to the problem of forward four-wave mixing. The first term on the right-hand side of Eq. (31) shows how the quantum fluctuations of the vacuum field are amplified by the four-wave-mixing process, whereas the second term shows how fields can be generated through quantum fluctuations of the material medium. Note that if we had simply quantized the semiclassical coupled amplitude equations describing forward four-wave mixing, only the first term of Eq. (31) would be present. Note further that our formalism gives us not only the quantities $\langle a^\dagger a\rangle$ and $\langle b^\dagger b\rangle$, that is, the mean number of photons in the signal and Stokes modes, but also the quantities $\langle ab\rangle$ and $\langle a^\dagger b^\dagger\rangle$, which describe the correlation between the signal and conjugate fields. These quantities can be used to calculate the amount of squeezing present in the output probe field.

For the purpose of calculating expectation values such as $\langle a\rangle$, $\langle ab\rangle$, and $\langle a^\dagger a\rangle$, it is not necessary to introduce a quasiprobability distribution such as the Wigner function. However, such functions are useful in the calculations of the higher-order statistical properties of the fields. For example, the calculation of intensity correla-

tions is greatly simplified through use of the properties of the linearized Fokker-Planck equation. For instance, we make use of the property that the Wigner function remains Gaussian at all subsequent times if it is Gaussian initially in the derivation of Eq. (45) below. This property is also useful in calculations of the higher-order squeezing exhibited by such systems. Elsewhere[21] it has also been shown how photon number distributions can be computed using Gaussian-distributed Wigner functions. Moreover, the Wigner function is quite attractive for the analysis of phase-sensitive noise since the Wigner function yields directly symmetrized expectation values. Of course, in principle any quasiprobability function can be used in performing the calculations and the end result must be the same. However, different distributions may look quite different and may diffuse quite differently. This property can be seen simply for the case of the parametric Hamiltonian $ga^\dagger b^\dagger + g^* ab$. Only the Wigner function has the attractive property that for such a Hamiltonian the system evolves on the classical trajectory.

In order to evaluate expressions (30) and (31) for the fields leaving the interaction volume, we set $t$ equal to $nL/c$, where $L$ is the length of the interaction region and $c/n$ is the phase velocity of propagation. For the present, we assume that the laser, signal, and conjugate fields propagate with the same phase velocity; wave-vector mismatch effects will be introduced below. It is convenient at this point to rewrite Eq. (31) in terms of dimensionless matrices $\mathcal{A}$ and $\mathcal{D}$ defined in terms of $A$ and $D$ through

$$\mathcal{A}=\frac{2A}{\alpha_0 c},\quad \mathcal{D}=\frac{2D}{\alpha_0 c}\ , \tag{32}$$

where $\alpha_0=4\pi n\omega\,|\,d\,|^2 T_2/\hbar c$ is the unsaturated, line-center absorption coefficient, so that Eq. (31) becomes

$$\langle \Psi(t)\Psi^\dagger(t)\rangle = \tfrac{1}{2}[\exp(\tfrac{1}{2}\alpha_0 L\mathcal{A})][\exp(\tfrac{1}{2}\alpha_0 L\mathcal{A})]^\dagger + \tfrac{1}{2}\alpha_0 L\int_0^1 dx\,\exp(\tfrac{1}{2}\alpha_0 L\mathcal{A}x)(2\mathcal{D}) \times\{\exp[(\tfrac{1}{2}\alpha_0 L\mathcal{A}x)]\}^\dagger\ . \tag{33}$$

This expression can be readily evaluated by introducing the matrix $S$ which diagonalizes $\mathcal{A}$,

$$\mathcal{A}=S^{-1}\begin{bmatrix}\lambda_1 & 0\\ 0 & \lambda_2\end{bmatrix}S\ . \tag{34}$$

In particular, the first term on the right-hand side of Eq. (33) can be evaluated using the laws of matrix multiplication and the expressions

$$[\exp(\tfrac{1}{2}\alpha_0 L\mathcal{A})]_{ij}=(S^{-1})_{i1}(S)_{1j}\exp(\tfrac{1}{2}\alpha_0 L\lambda_1) + (S^{-1})_{i2}(S)_{2j}\exp(\tfrac{1}{2}\alpha_0 L\lambda_2)\ , \tag{35a}$$

$$\{[\exp(\tfrac{1}{2}\alpha_0 L\mathcal{A})]^\dagger\}_{ij}=[\exp(\tfrac{1}{2}\alpha_0 L\mathcal{A})]^*_{ji} = (S^{-1})^*_{j1}(S)^*_{1i}\exp(\tfrac{1}{2}\alpha_0 L\lambda_1^*) + (S^{-1})^*_{j2}(S)^*_{2i}\exp(\tfrac{1}{2}\alpha_0 L\lambda_2^*)\ . \tag{35b}$$

In addition, by performing the integration indicated in the second term of Eq. (32) one finds that the $i,j$ matrix element of the second term is given by

$$\sum_{kl}(\tfrac{1}{2}\alpha_0 L)(2D)_{kl}\left[(S^{-1})_{i1}(S)_{1k}(S^{-1})^*_{j1}(S)^*_{1l}\frac{\exp[(\frac{1}{2}\alpha_0 L)(\lambda_1+\lambda_1^*)]-1}{\frac{1}{2}\alpha_0 L(\lambda_1+\lambda_1^*)}\right.$$
$$+(S^{-1})_{i2}(S)_{2k}(S^{-1})^*_{j1}(S)^*_{1l}\frac{\exp[(\frac{1}{2}\alpha_0 L)(\lambda_2+\lambda_1^*)]-1}{\frac{1}{2}\alpha_0 L(\lambda_2+\lambda_1^*)}+(S^{-1})_{i1}(S)_{1k}(S^{-1})^*_{j2}(S)^*_{2l}\frac{\exp[(\frac{1}{2}\alpha_0 L)(\lambda_1+\lambda_2^*)]-1}{\frac{1}{2}\alpha_0 L(\lambda_1+\lambda_2^*)}$$
$$\left.+(S^{-1})_{i2}(S)_{2k}(S^{-1})^*_{j2}(S)^*_{2l}\frac{\exp[(\frac{1}{2}\alpha_0 L)(\lambda_2+\lambda_2^*)]-1}{\frac{1}{2}\alpha_0 L(\lambda_2+\lambda_2^*)}\right]\ . \tag{36}$$

Phase-mismatch effects are included in the theory through the exponential phase factor $\exp[-it(2\omega-\omega_s-\omega_c)]$ that appears in Eq. (23). For the case in which the refractive indices ($n$, $n_c$, and $n_s$) of the three waves are not equal, this term when transformed to spatial dependence becomes

$$\exp[-iz(2n\omega/c-n_c\omega_c/c-n_s\omega_s/c)]=\exp(-iz\,\Delta k)\ ,$$

where $\Delta k=2k-k_c-k_s$. Equation (23) can be solved even in the presence of the phase-mismatch term. The solution is still given by Eqs. (32)–(35) but with $\mathcal{A}$ replaced by

$$\mathcal{A}-\frac{2i\,\Delta k}{\alpha_0}\begin{bmatrix}0 & 0\\ 0 & -1\end{bmatrix}\ . \tag{37}$$

## III. NUMERICAL RESULTS

In this section, the formulas derived in Sec. II are evaluated numerically and are displayed graphically for several cases of interest. In Fig. 1, we consider the case of a radiatively broadened medium (i.e., $T_2/T_1=2$) excited by a pump laser that is tuned to line center ($\Delta=0$) and has a field strength such that the normalized Rabi frequency $\Omega T_2$ is equal to 16. We assume perfect phase matching, that is, $\Delta k=0$. The mean number of photons $\langle n\rangle=\langle a^\dagger a\rangle$ generated at the signal frequency $\omega_s$ is plotted in this figure as a function of the signal frequency $\omega_s$ for several different values of the absorption path length $\alpha_0 L$ through the atomic medium. For the case of a short medium ($\alpha_0 L=0.01$), the emission line shape is identical

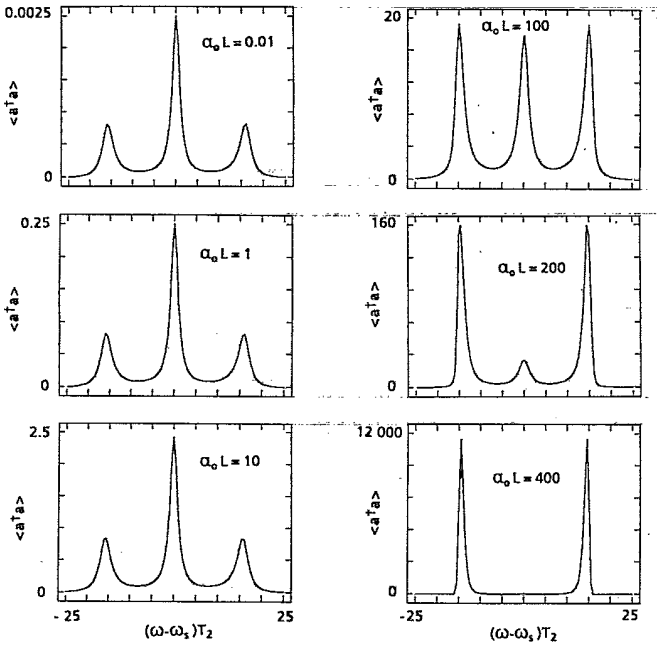


FIG. 1. Mean number of photons per mode $\langle n \rangle = \langle a^\dagger a \rangle$ radiated at frequency $\omega_s$ plotted as a function of detuning from the laser frequency $\omega$ for several different values of the unsaturated, line-center, intensity absorption path length $\alpha_0 L$. The calculation assumes the case of a radiatively broadened transition ($T_2/T_1 = 2$), that the laser is tuned to the center of the absorption line ($\Delta = 0$), that the normalized Rabi frequency associated with the laser field strength is $\Omega T_2 = 16$, and the case of perfect phase matching ($\Delta k = 0$).

to the well-known resonance fluorescence line shape. However, as the path length through the medium is increased the predicted line shape becomes significantly modified. In particular, the number of photons per mode increases rapidly with propagation distance, especially for signal modes near the Rabi sideband frequencies. In addition, the Rabi sidebands become more prominent as the path length is increased, whereas the central component is strongest for the case of short path lengths. Moreover, the Rabi sidebands are seen to display gain narrowing, that is, the width of the sideband decreases with increasing propagation distance.

It is instructive to see how the formalism developed here predicts a spectrum that reduces to the Mollow spectrum in the limit of short propagation lengths. Retaining only terms to lowest order in $t$, Eq. (31) becomes

$$\frac{\langle a^\dagger a \rangle}{t} = \tfrac{1}{2}(A_{11} + A_{11}^*) + 2D \ , \tag{38}$$

which on using (28) and (29) becomes

$$\frac{\langle a^\dagger a \rangle}{t} = \frac{N}{2\hbar^2} |\beta_s|^2 \{ [Q_{ss}^{+-}(i\nu_s) - C_{ss}^{+-}(i\nu_s)] + \text{c.c.} \} \ . \tag{39}$$

If we now introduce the definitions (11), (12), and (17), Eq. (39) reduces to

$$\frac{\langle a^\dagger a \rangle}{t} \propto \text{Re} \lim_{t \to \infty} \int_0^\infty d\tau e^{i\nu_s \tau} \times [\langle s^+(t+\tau) s^-(t) \rangle - \langle s^\dagger(t+\tau) \rangle \langle s^-(t) \rangle] \ . \tag{40}$$

(40) is in fact the standard part of the Mollow spectrum written in terms of the atomic correlation functions. Note further that the right-hand side of (39) is just $(A_1 + A_1^*)$ in the notation of Holm and Sargent.[13]

The dependence of the width and height of the Rabi sidebands on the propagation path length for the case of radiative broadening and central tuning of the pump laser is summarized in Fig. 2 for several different values of the Rabi frequency associated with the laser field strength. For each case shown in Fig. 2(a), the mean number of photons per mode at the peak of the Rabi sideband is seen to increase linearly with propagation distance for short media and to increase much more rapidly for longer media. The linear increase occurs when the emission occurs predominantly by spontaneous emission, whereas the more rapid growth occurs once the stimulated processes which lead to exponential gain due to four-wave-mixing effects become important. In Fig. 2(b), the linewidth (full width at half maximum) of either of the sidebands is shown plotted as a function of the propagation path length. Significant gain narrowing of the sidebands is predicted.

The nature of the solution is qualitatively somewhat different for the case of a pump laser that is detuned from the atomic resonance. The case of a detuned pump laser ($\Delta T_2 = -8$) and perfect phase matching is shown in Fig. 3 for a radiatively broadened medium ($T_2/T_1 = 2$) and in Fig. 4 for a medium in which the broadening is dominated by collisions ($T_2/T_1 = 0.02$). For a short medium ($\alpha_0 L = 0.01$) the spectra are again those of conventional resonance fluorescence, with two sidebands separated from the central component by the generalized Rabi frequency

$$\Omega' = (\Omega^2 + \Delta^2)^{1/2} \ . \tag{41}$$

For the radiatively broadened medium the two sidebands

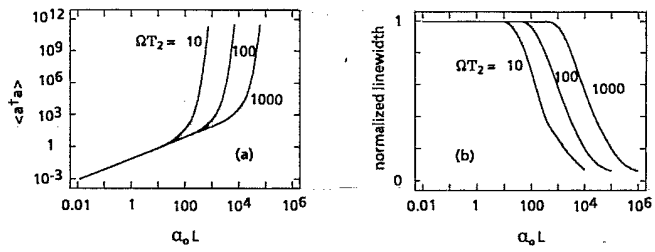


FIG. 2. Mean number of photons per mode at the peak of either of the Rabi sidebands (a) and the width of the Rabi sideband normalized by its width in the limit of small $\alpha_0 L$ (b) plotted as functions of the absorption path length through the interaction region for several different values of the laser Rabi frequency. The calculation assumes the case of a radiatively broadened transition, that the laser frequency is tuned to line center, and that $\Delta k = 0$.

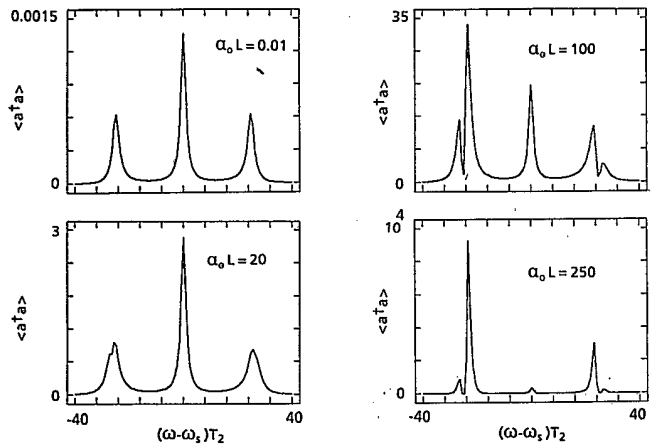


FIG. 3. Mean number of photons per mode radiated at frequency $\omega_s$ plotted as a function of the detuning from the laser frequency $\omega$ for several different values of the absorption path length. The calculation assumes the case of a radiatively broadened medium, that the laser frequency is detuned from line center such that $\Delta T_2 = -8$, that $\Omega' T_2 = 25$, and that $\Delta k = 0$.

are of equal height, whereas for the collisionally broadened medium collisional redistribution effects[22] lead to an enhancement of the sideband closer to the atomic resonance frequency. For longer values of the propagation path length, four-wave-mixing processes become important. These processes lead to exponential growth of the signal and conjugate fields. For both the radiatively and collisionally broadened media, the Rabi sideband that is further from the atomic resonance frequency has the higher intensity. The reason why this sideband is higher is that it experiences gain due to both the stimulated three-photon effect[23] and the parametric mixing process. Conversely, the other sideband (the one closer to the atomic resonance frequency) experiences loss due to the atomic absorption but gain due to the parametric mixing process. The dip in the spectra within the sidebands exactly at the Rabi sideband frequency occurs because in the presence of perfect phase matching the coupling between the two sidebands is so strong that the loss

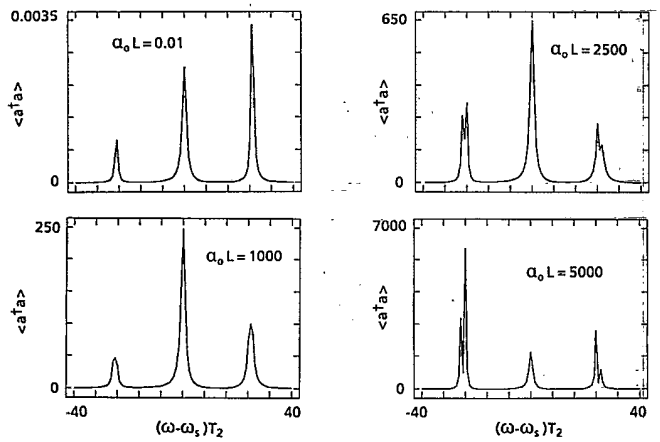


FIG. 4. Same as Fig. 3, but for the case of a medium for which the broadening is largely collisional such that $T_2/T_1 = 0.02$.

at one sideband quenches the gain at the other, leading to decreased gain for the coupled solution. These features of the solution are analogous to those that appear in the semiclassical treatment.[4]

We have investigated the role of phase-matching effects by considering how $\langle n \rangle = \langle a^\dagger a \rangle$ at each of the Rabi sideband frequencies depends upon $\Delta k$ for one of the cases shown in Fig. 4, in particular, the case $T_2/T_1 = 0.02$, $\Delta T_2 = -8$, $\Omega' T_2 = 25$, and $\alpha_0 L = 2500$. Figure 5(a) shows that the output at $\delta\omega = (\omega - \omega_s)T_2 = -25$ is minimized for the case of perfect phase matching. The reason is that this sideband experiences gain due to the stimulated three-photon effect, and hence its height is increased by decoupling it from the other (lossy) sideband through a large phase mismatch. Figure 5(b) shows how the output at $\delta\omega = +25$ depends upon the wave-vector mismatch. In this case the output is maximized by coupling the sideband strongly but not too strongly to the other sideband, that is, through the use of a small not nonzero value of $\Delta k$.

We have also investigated the relative importance of the two contributions to the output signal represented by the first and second terms on the right-hand side of Eq. (31). For the case of a collisionally broadened medium with $T_2/T_1 = 0.02$, the contribution of the second term is at least 100 times greater than that of the first term for all of the cases we have examined. Hence in this limit in which the dephasing is dominated by collisions, the four-wave-mixing process is initiated primarily by fluctuations of the atomic dipoles and not by quantum fluctuations of the incident vacuum field. The case of a radiatively broadened medium is more complicated. Figure 6 shows the contributions from the two terms in Eq. (31) and their sum for two representative cases. For the example shown in Fig. 6(a) the two contributions are roughly equal in magnitude, whereas for the example shown in Fig. 6(b) the contribution due to fluctuations in the material response exceeds the contribution due to fluctuations in the radiation field by approximately a factor of 10. We have found no examples with $T_2/T_1 = 2$ for which the first term makes the dominant contribution nor have we found examples where the first term is negligibly small. Hence it appears that for a radiatively broadened medium both field and material fluctuations are important in initiating the four-wave-mixing process.

We have also examined the statistical properties of the transmitted fields to determine the extent to which the output constitutes a squeezed state of the field. We define

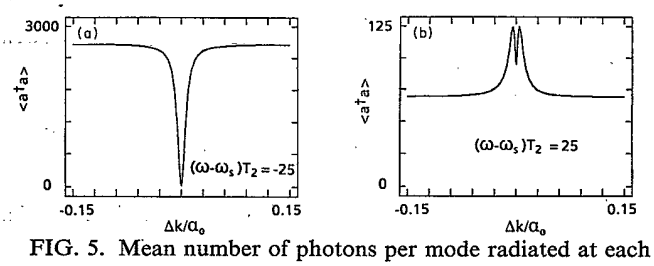


FIG. 5. Mean number of photons per mode radiated at each of the Rabi sidebands plotted as a function of the normalized wave-vector mismatch $\Delta k$ for the case $T_2/T_1 = 0.02$, $\Delta T_2 = -8$, and $\alpha_0 L = 2500$.

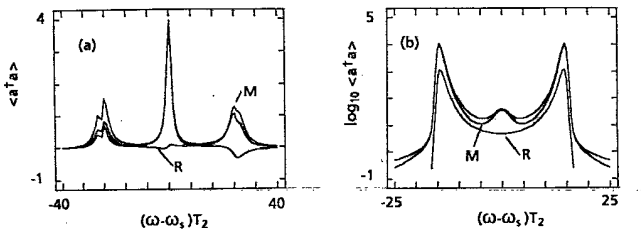


FIG. 6. Mean number of photons per mode radiated at frequency $\omega_s$ plotted as a function of the detuning from the laser frequency $\omega$. In each plot, the curve marked $R$ gives the contribution of the first term in Eq. (31) whose origin is fluctuations in the incident vacuum radiation field, and the curve marked $M$ gives the contribution of the second term in Eq. (31) whose origin is fluctuations in the atomic dipoles that constitute the material system. Plot (a) corresponds to the case $T_2/T_1=2$, $\Delta T_2=-8$, $\Omega' T_2=25$, $\alpha_0 L=20$, and $\Delta k=0$, and plot (b) corresponds to the case $T_2/T_1=2$, $\Delta T_2=0$, $\Omega' T_2=16$, $\alpha_0 L=400$, and $\Delta k=0$.

the squeezing parameter as[15]

$$S=\tfrac{1}{2}[\langle a^\dagger a\rangle+\langle b^\dagger b\rangle+2\,\mathrm{Re}(\langle ab\rangle e^{i\theta})]\ , \tag{42}$$

where $\theta$ denotes the phase angle of the linear combination of the signal and conjugate modes. The squeezing parameter is defined in such a manner that $S$ is equal to 0 for a coherent state and is equal to $-1$ for a state possessing perfect squeezing; any state with a negative value of $S$ is said to be a squeezed state. It is convenient to introduce the maximum-squeezing parameter

$$S_{\max}=\tfrac{1}{2}(\langle a^\dagger a\rangle+\langle b^\dagger b\rangle-2\,|\langle ab\rangle|) \tag{43}$$

as the maximum value that $S$ attains as $\theta$ is varied. Figure 7 shows the spectrum of the maximum-squeezing parameter for several different propagation path lengths for the case $T_2/T_1=2$, $\Delta T_2=-8$, and $\Omega' T_2=25$, that is, the same case for which the emission spectrum was displayed in Fig. 3. In all four cases broad regions of squeezing centered about the Rabi sideband frequency are predicted. For the shortest interaction path length shown, the amount of squeezing is probably too small to be measurable. However, in the other cases appreciable levels of squeezing are predicted. It should be noted that several authors have produced squeezed light by using four-wave mixing[24,25] in situations where the pump was far detuned from the atomic resonance and the pump intensity was much less than the saturation intensity. In the present paper we are discussing a very different regime. We have also studied the case of a centrally tuned laser for $T_2/T_1=2$, $\Omega T_2=16$, and $\Delta k=0$, and find that no squeezing is predicted for any value of $\alpha_0 L$. In addition, we have investigated collisional media with $T_2/T_1=0.02$, and have found no case in which squeezing is predicted.

Finally, the higher-order correlation characteristics of the generated fields can also be studied by using the Gaussian property of the Wigner distribution function. In particular, we can show that the fields at the two sidemodes are strongly correlated with each other. To see this we calculate the correlation function

$$C_{ab}=\langle a^\dagger a b^\dagger b\rangle-\langle a^\dagger a\rangle\langle b^\dagger b\rangle\ , \tag{44}$$

which on using the Gaussian property of the Wigner function reduces to

$$C_{ab}=|\langle ab\rangle|^2\ . \tag{45}$$

This function is plotted in Fig. 8 for the same choice of parameters for which squeezing was predicted in Fig. 7. In each case shown, a strong correlation is predicted for the radiation at the two Rabi sidebands. Strong correlation is predicted even in the case of a short interaction region ($\alpha_0 L=0.01$), for which case the mean number of photons per mode $\langle a^\dagger a\rangle$ is quite small (see Fig. 3). Since the photons are produced in pairs, once a photon is detected in mode $a$ the probability of detecting a second photon in mode $b$ is quite large. The correlation could be measured experimentally either by separating the two sidebands spectrally before measuring their intensities or by performing the experiment in a relatively dense atomic vapor in which case the two sidebands would be emitted in different directions due to phase-matching effects.

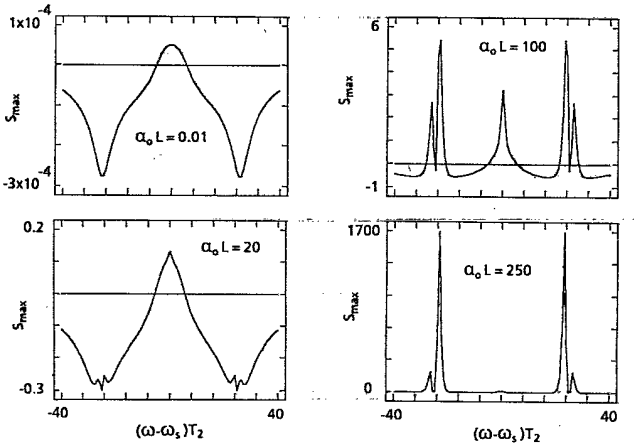


FIG. 7. Maximum-squeezing parameter plotted as a function of the detuning $\omega-\omega_s$ for the case $T_2/T_1=2$, $\Delta T_2=-8$, $\Omega' T_2=25$, $\Delta k=0$, and for several different values of the absorption pathlength $\alpha_0 L$.

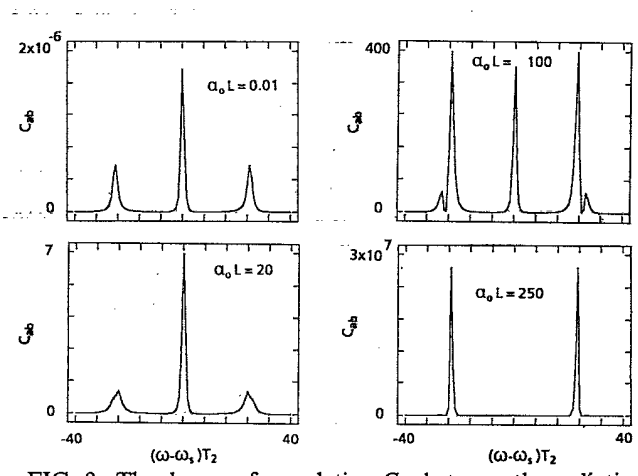


FIG. 8. The degree of correlation $C_{ab}$ between the radiation at frequencies $\omega_s$ and $\omega_c=2\omega-2\omega_s$ plotted as a function of $\omega-\omega_s$ for the same cases shown in Fig. 7.

## IV. CONCLUSIONS

We have presented an analysis of Rabi sideband generation by forward four-wave mixing in a homogeneously broadened atomic medium in the two-level approximation. This treatment is fully quantum mechanical and shows how the four-wave-mixing process is initiated by quantum noise. As the propagation path length through the medium is increased, the spectrum of the radiation emitted in the forward direction evolves continuously from that of spontaneous emission from a strongly driven atom (resonance fluorescence) to that characteristic of a four-wave-mixing process. The treatment is based on the use of the Wigner distribution function, and is thus capable of separating the process into a part initiated by quantum fluctuations of the incident vacuum radiation field and a part initiated by fluctuations of the atomic dipoles. Both of these contributions are important for a radiatively broadened medium, whereas only the material fluctuations are important for a medium in which the broadening is predominantly collisional. Our treatment predicts that certain superpositions of the radiation generated within the medium constitute a squeezed state of the optical field for the case of a radiatively broadened medium for certain values of the laser detuning and intensity, and that under these same conditions strong correlation between the radiation at the two sidebands occurs.

## ACKNOWLEDGMENTS

We gratefully acknowledge the support of a National Science Foundation (NSF) travel grant which has allowed each of us to visit the other at his home institution. The portion of the work performed at the University of Rochester was supported by the U.S. Army Research Office and the U.S. Office of Naval Research.

[1]B. R. Mollow, Phys. Rev. **188**, 1969 (1969).
[2]F. Schuda, C. R. Stroud, Jr., and M. Hercher, J. Phys. B **7**, L198 (1974).
[3]B. R. Mollow, Phys. Rev. A **7**, 1319 (1973).
[4]R. W. Boyd, M. G. Raymer, P. Narum, and D. J. Harter, Phys. Rev. A **24**, 411 (1981).
[5]C. H. Skinner and P. D. Kleiber, Phys. Rev. A **25**, 151 (1979).
[6]Y. H. Meyer, Opt. Commun. **34**, 434 (1980).
[7]G. Brechignac, Ph. Cahuzac, and A. Debarre, Opt. Commun. **35**, 87 (1980).
[8]D. J. Harter, P. Narum, M. G. Raymer, and R. W. Boyd, Phys. Rev. Lett. **46**, 1192 (1981).
[9]D. J. Harter and R. W. Boyd, Phys. Rev. A **29**, 739 (1984).
[10]J. Krasinski, D. J. Gauthier, M. S. Malcuit, and R. W. Boyd, Opt. Commun. **54**, 241 (1985).
[11]M. Sargent III, D. A. Holm, and M. S. Zubairy, Phys. Rev. A **31**, 3112 (1985).
[12]S. Stenholm, D. A. Holm, and M. Sargent III, Phys. Rev. A **31**, 3124 (1985); D. A. Holm and M. Sargent III, *ibid.* **35**, 2150 (1987).
[13]D. Holm and M. Sargent III, Phys. Rev. A **33**, 4001 (1986).
[14]M. D. Reid and D. F. Walls, Phys. Rev. A **31**, 3124 (1985); **33**, 4465 (1986).
[15]M. D. Reid and D. F. Walls, Phys. Rev. A **34**, 4929 (1986).
[16]G. S. Agarwal, Phys. Rev. A **34**, 4055 (1986).
[17]F. Castelli, L. A. Lugiato, and M. Vadacchino, Nuovo Cimento D (to be published), have discussed the squeezing produced by a system of atoms within a bistable cavity. Their results for squeezing in the "bad-cavity limit" are very similar to our results.
[18]G. S. Agarwal, Phys. Rev. A **33**, 2472 (1986); D. F. Walls, Nature (London) **306**, 141 (1983).
[19]M. J. Collet, D. F. Walls, and P. Zoller, Opt. Commun. **52**, 145 (1984).
[20]Our basic equation (8) is equivalent to Eq. (100) of Sargent *et al.* (Ref. 11) and to Eq. (26) of Reid and Walls (Ref. 15). These latter authors have already established the equivalence of their equation to that of Sargent *et al.* We find that our Eq. (8) is equivalent to that of Sargent *et al.* and that the quantities $A_1$, $B_1$, $C_3$, and $D_3$ that appear in their expression are related to our correlation functions through

$$A_1=\frac{|\beta_s|^2N}{2\hbar^2}[Q_{ss}^{+-}(i\nu_s)-\hat{C}_{ss}^{+-}(i\nu_s)]\ ,$$

$$B_1=\frac{|\beta_s|^2N}{2\hbar^2}[Q_{ss}^{+-}(i\nu_s)+\hat{C}_{ss}^{+-}(i\nu_s)]\ ,$$

$$C_3=-\frac{\beta_s^*\beta_c^*N}{2\hbar^2}[(\hat{Q}_{cs}^{++}(-i\nu_s)+\hat{C}_{cs}^{++}(-i\nu_s)]\ ,$$

$$D_3=-\frac{\beta_s^*\beta_c^*N}{2\hbar^2}[(\hat{Q}_{cs}^{++}(-i\nu_s)-\hat{C}_{cs}^{++}(-i\nu_s)]\ .$$

Although our starting equations are equivalent, we have been able to reproduce the numerical results shown in Fig. 3 of Ref. 13 only when we use values of the intensity and propagation distance that differ from those quoted in the figure caption. The authors of this article have informed us that in fact the figure caption is incorrect, and that the curves correspond to intensities twice as great and propagation distances twice as large as those quoted in the caption.
[21]G. S. Agarwal and G. Adam, Phys. Rev. A **38**, 750 (1988).
[22]J. L. Carlsten, A. Szöke, and M. G. Raymer, Phys. Rev. A **15**, 1029 (1977).
[23]C. Cohen Tanoudji and S. Reynaud, J. Phys. B **100**, 345 (1977).
[24]R. E. Slusher, L. W. Hollberg, B. Yurke, J. C. Mertz, and J. F. Valley, Phys. Rev. Lett. **55**, 2409 (1985).
[25]M. W. Maeda, P. Kumar, and J. H. Shapiro, Opt. Lett. **12**, 161 (1987); these experimental results are interpreted in terms of S. T. Ho, P. Kumar, and J. H. Shapiro, Phys. Rev. A **35**, 3982 (1987).